ARTICLE

Mesogenic $[Rh(L)_4](A)$ Complexes Form Mesophases with $Rh^I\cdots Rh^I$-Containing and Triphenylene-Discotic Segregated Columns. Effect of $Rh^I\cdots Rh^I$ Interactions and $A^- = [Au(CN)_2]^-$ on Hole Mobility

Received 00th January 20xx,
Accepted 00th January 20xx

DOI: 10.1039/x0xx00000x

Verónica Conejo-Rodríguez,[a] Bertrand Donnio,*[b] Benoît Heinrich,[b] Roberto Termine,[c] Attilio Golemme[c] and Pablo Espinet*[a]

Rh^I complexes $[Rh(L)_4](A)$ ($A^- = Cl^-$, BF_4^-, $[Au(CN)_2]^-$) with conventional arylisocyanides (*p*-$MeC_6H_4(NC)$, L^A; *p*-$MeOC_6H_4(NC)$, L^B; 3,5-$(OMe)_2C_6H_3(NC)$, L^C) or with the alkoxy-functionalized triphenylene-arylisocyanides $TPh(OC_{12}H_{25})_5(O(CH_2)_6OC_6H_4(NC)$-*p*) (**$L^{D1}$**) and $TPh(OC_{12}H_{25})_5(O(CH_2)_6OC_6H_2Me_2(NC)$-*p*) (**$L^{D2}$**), have been prepared and their self-assembly, aggregation, optical, redox, mesogenic and conducting properties investigated. Intermolecular π-π stacking, $Rh^I\cdots Rh^I$, and $Rh^I\cdots Au^I$ interactions rule the crystal packing and aggregation in solution for the complexes with L^A, L^B, and L^C. For the complexes with the alkoxy-functionalized-triphenylene isocyanides **L^{D1}** and **L^{D2}** Rh^I mesogenic behaviour is induced, giving rise to multicolumnar mesophases in broad temperature ranges (*ca*. 70-160 °C). Detailed analysis (POM, DSC, S/WAXS and GIWAXS) of the columnar mesophases has allowed us to propose precise packing models that explain the diverse supramolecular arrangements found in the nanostructured condensed phases. Columnar alignments predominantly with Rh···Rh (or Rh···Au for **L^{D2}** in specific conditions) interactions are observed, depending on the aligning conditions. The hole mobility in the columnar mesophases of the complexes with Rh···Rh interactions are ~1 $cm^2\ V^{-1}\ s^{-1}$, that is up to four orders of magnitude higher than those reported for columnar mesophases of organic triphenylene derivatives, and increases still one order of magnitude in the mesophases containing the $[Au(CN)_2]^-$ counteranion.

Introduction

Since early studies in the 1970's, stable d^8 square-planar rhodium(I) complexes $[Rh(CNAr)_4](A)$ (Ar = aryl; A^- = anion) have been reported.[1] Many of them show a natural tendency to establish homometallic interactions, forming $[Rh(CNAr)_4]_n^{n+}$ oligomers (n = 1, 2, 3 …) in the solid state and in concentrated solutions in spite of the repulsive contribution of identical positive charges. Stabilizing π-π interactions overcome this electrostatic repulsion and give rise to Rh···Rh orbital interactions at distances significantly shorter than the sum of vdW radii. The contribution to oligomer stability of these Rh···Rh orbital interactions (about 10-15% of the total stabilizing forces) is relatively small compared to the π-π interactions,[2] but it is responsible for the remarkable photophysical properties that these polynuclear complexes exhibit.[3] The appropriate combination of metal-metal interactions with other (donor-acceptor, hydrophobic-hydrophilic, cation-anion) attractive interactions facilitates the design of a vast range of functional nanomaterials such as sensors, nanowires, or ionic liquids.[3b,46]

For a different reason, $(Q)[Au(CN)_2]$ (Q^+ = cation) d^{10} complexes give also rise to oligomeric complexes with Au···Au interactions. In this case, where aryls are absent, it is the aurophilic interactions that help to overcome the electrostatic repulsion between anions.[7,8] Speaking in general, there is a multitude of studies of luminescent materials based on the presence of Au···Au aurophilic interactions, including our recent report of gold complexes that are non-luminescent solid materials but give rise to luminescent mesophases upon melting or grinding the solid.[9]

Surprisingly, the synthetic possibility of combining $[Au(CN)_2]^-$ and $[Rh(CNAr)_4]^+$ complexes in molecular systems, which might facilitate the formation of compounds with Rh···Au interactions by cation-anion electrostatic attraction, had apparently been disregarded**.** Our group recently published a mixed $[Rh(CNXylyl)_4][Au(CN)_2]$ system, in which the contribution of the anion-cation attractive forces between d^8 $[Rh(CNXylyl)_4]^+$ and d^{10} $[Au(CN)_2]^-$ gives rise, in the solid state, to different crystals (sometimes different polymorphs) displaying $d^8\cdots d^{10}$ short distances. The accidental choice of the commercial CNXylyl (**L^X**, Chart 1) as ligand for this system was fortunate because the presence of two *ortho* Me groups in this isocyanide induces some reluctance to the formation of the multiple intra-unit π-π stackings observed in other $[Rh(CNAr)_4]^+$ cationic units and leads instead to the formation of polymetallic arrangements where Rh···Au interactions are preferred (Figure 1).[10] This interesting and rich solid state behaviour has prompted us to explore further these two metallic systems and their binary combination in the design of metal-containing thermotropic liquid crystals (metallomesogens).[11,12] Their observed tendency to create M···M interactions in concentrated solutions and in the solid state looks promising for building potentially columnar semiconductor mesophases with separate channels for the transport of charges, holes or electrons. To this end we have chosen the triphenylene unit (TPh), conveniently

[a] *IU CINQUIMA/Química Inorgánica, Facultad de Ciencias, Universidad de Valladolid, E-47071 Valladolid, Spain.*
[b] *Institut de Physique et Chimie des Matériaux de Strasbourg (IPCMS), UMR 7504 (CNRS-Université de Strasbourg), F-67034 Strasbourg Cedex 2, France.*
[c] *LASCAMM CR-INSTM, CNR-Nanotec, Dipartimento di Fisica, 87036 Rende, Italy.*
Electronic Supplementary Information (ESI) available: Synthesis and chemical characterisation details, UV-Visible and electrochemical data, POM, DSC S/WAXS and GIWAXS and hole mobility studies on the mesophases. See DOI: 10.1039/x0xx00000x

functionalized with lateral aliphatic chains, as a powerful inductor of columnar mesophases.

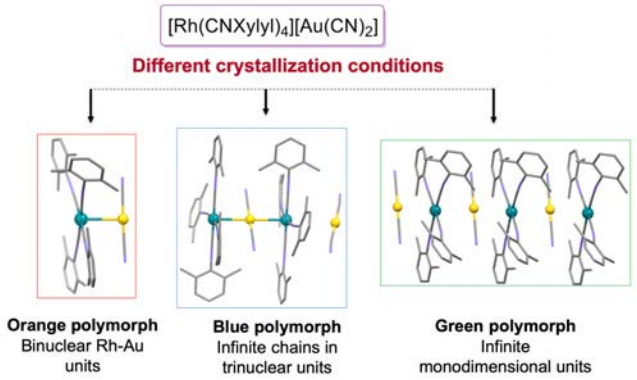

Figure 1. Examples of different crystal polymorphs of $[Rh(CNXylyl)_4][Au(CN)_2]$ with Rh···Au interactions.[10]

Triphenylene offers many possibilities of functionalization around its core. This has yielded a wide variety of materials self-assembling into many types of columnar mesophases,[13,14,15,16] and having different applications in several fields.[13,17,18,19] Compared to the many reports of TPh organic liquid crystals, studies on metallomesogens containing triphenylene derivatives are scarce.[20,21,22] In the last years we have published a few studies on diverse liquid crystals using metalorganic triphenylene systems,[23] very different from those proposed here.

Results and Discussion

Synthesis and Characterization of the arylisocyanide ligands

In this work we pursue the synthesis of Rh^{I} columnar metallomesogens $[Rh(L)_4](A)$ ($A^- = Cl^-$, BF_4^-; L = aryl isocyanide) with Rh···Rh interactions as potentially flexible monodimensional conductors. We use the triphenylene moiety (TPh) to support the aryl isocyanide moiety that has to coordinate to Rh. Three conventional arylisocyanide ligands with no substituent at the *ortho* position, **L^{A-C}**, are used as simpler models of the triphenyleneisocyanide ligand **L^{D1}** (Chart 1), to obtain information on self-assembling of Rh centres. In addition, **L^{X}** is considered a model of the triphenyleneisocyanide derivative with **L^{D2}**. According to our previous solid state results with **L^{X}** (Figure 2),[10] for $A^- = [Au(CN)_2]^-$, Rh···Au interactions in the mesophase might be more likely with **L^{D2}** than with **L^{D1}**.

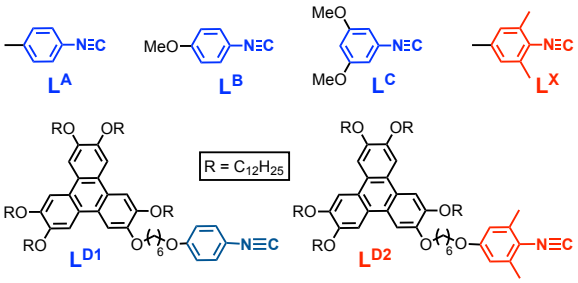

Chart 1. Arylisocyanide **L^{A,B,C,X}** and triphenyleneisocyanide **L^{D1}** and **L^{D2}** ligands used in this work.

The arylisocyanide and triphenyleneisocyanide ligands were prepared using modified literature methods.[8a,23d,24] The unreported triphenyleneisocyanide ligand **6** (**L^{D2}**) was synthesized as shown in Scheme 1.

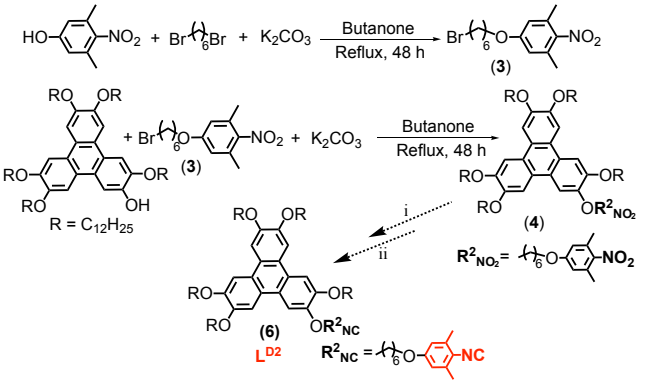

Scheme 1. Synthesis of **L^{D2}**: i) Sn, formic acid, toluene, reflux 3 h; ii) triphosgene, Et_3N, dry CH_2Cl_2, 0-25 ºC. See ESI.

The ^1H NMR spectra are very similar for all the *p*-substituted isocyanides. In ligands L^A, L^B and **L^{D1}** they show the expected AA´XX´ spin system for the aryl protons of the isocyanide group. An AB_2 spin system is observed for L^X, and a singlet for **L^{D2}**. In the case of the *m*-substituted ligand (L^C) a triplet for the *ortho*- and a doublet for the *para*-H atoms, and a broad singlet for the two methoxy groups, are observed. The aryl protons of the triphenylene core provide a singlet. For the methylene groups, a multiplet and a triplet are observed in the range 4.2–3.9 ppm, corresponding to the first methylene group of the alkyloxy moieties. The remaining chain hydrogen atoms appear overlapped in the range 1.9–1.3 ppm. Singlets for the Me/MeO groups are also observed (see ESI). The IR spectra show a broad band corresponding to ν(C≡N) in the range 2112-2135 cm^{-1}.

Synthesis and Characterization of $[Rh(L)_4](A)$ Model and Mesogenic arylisocyanide Complexes.

The reaction of 8 equivalents of ligands **L^{A}**-**L^{D1}** with $[RhCl(COD)]_2$ (COD = 1,5-cyclooctadiene) in dichloromethane (Scheme 2) led, as reported for related systems,[1d,3b,4–6] to the corresponding $[Rh(L)_4](Cl)$ complexes **7**-**10**. The complexes $[Rh(L)_4](BF_4)$ (**11**-**15**) were synthesized from $[Rh(COD)_2](BF_4)$ and 4 equivalents of the corresponding isocyanide. Finally the corresponding heterobimetallic complexes $[Rh(L)_4][Au(CN)_2]$ (**16**-**20**) were obtained by metathesis of the BF_4 complexes with $(K)[Au(CN)_2]$. The complex with **L^{X}** has been reported previously.[25]

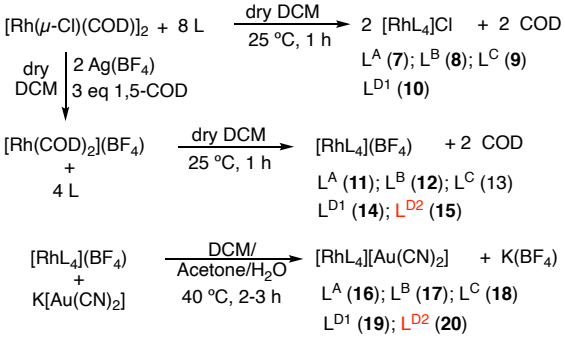

Scheme 2. Synthesis of $[RhL_4](A)$ complexes.

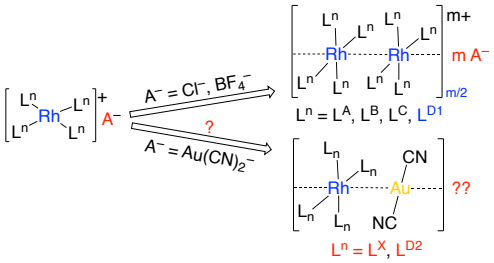

Figure 2. Possible M···M interactions in the solid, or in possible mesophases of complexes with promesogenic $\mathbf{L^{D1}}$ and $\mathbf{L^{D2}}$.

For complexes with ligand $\mathbf{L^{D2}}$, an equilibrium mixture of [RhCl($\mathbf{L^{D2}}$)$_3$] and [Rh($\mathbf{L^{D2}}$)$_4$](Cl) was formed, as observed previously for the xylylisocyanide ligand L^X.[1d] In the case of $\mathbf{L^{D2}}$, the problem could not be solved using an excess of $\mathbf{L^{D2}}$ to displace the equilibrium, as we did for L^X, because the mixture of excess ligand and complex [Rh($\mathbf{L^{D2}}$)$_4$](Cl) could not be separated.

In the ^{1}H NMR spectra of the complexes, the aromatic protons *ortho* to the isocyanide group show a slight deshielding upon coordination to Rh^I, as reported for other related compounds.[8a] The OCH_2 protons appear at *ca.* 4 ppm, and the rest of the alkyl protons are seen in the 1.94–0.88 ppm range. The solid state IR spectra of all the complexes exhibit stretching ν(C≡N) isocyanide absorptions at higher wavenumbers than in the corresponding free ligands: 40–36 cm^{-1} higher for the Rh^I complexes without methyl groups in *ortho* position and 27–22 cm^{-1} higher for the Rh^I complexes of L^X and $\mathbf{L^{D2}}$, with methyl groups in *ortho* position (Table 1). All these bands appear in the complexes in the range 2129-2160 cm^{-1} and are broad. For this reason, they are likely overlapping the weaker $\nu(C{\equiv}N)_{cyanide}$ absorptions in the [Rh(L)$_4$][Au(CN)$_2$] complexes (ν(C≡N) for K[Au(CN)$_2$] appears at 2150 cm^{-1}). In the absence of independent observation, the similarity of all band positions for all the [Rh(L)$_4$](A) complexes might be consistent with a common cation and suggesting that the [Au(CN)$_2$]$^-$ moiety is not involved in formation of Rh···Au···Rh interactions in the solids. Other observations discussed later suggest the same.

Table 1. IR ν(C≡N) isocyanide bands (cm^{-1}) for free and coordinated isocyanide ligands.

L / $\nu_{C\equiv N}$ free	$\nu_{C\equiv N}$ coordinated		
	[Rh(L)$_4$](Cl)	[Rh(L)$_4$](BF$_4$)	[Rh(L)$_4$] [Au(CN)$_2$]
$\mathbf{L^A}$ / 2125	2141	2150	2142
$\mathbf{L^B}$ / 2123	2139	2140	2151
$\mathbf{L^C}$ / 2134	2151	2158	2152
L^X / 2109	2129*	2129**	2133**
$\mathbf{L^{D1}}$ / 2120	2160	2156	2157
$\mathbf{L^{D2}}$ / 2112	2134	2139	2139

ATR measurements. *Data from reference 4. **Data from reference 10.

Attempts at growing single crystals suitable for X-ray diffraction provided some solid-state structures of the model complexes. Deep blue single crystals of [Rh(L^C)$_4$](Cl) (**9**), obtained by slow diffusion of hexane into a diluted solution in CH_2Cl_2 of the blue solid obtained in the synthesis, provided the structure depicted in Figure 3, with a polymeric arrangement of the Rh atoms and Rh···Rh = 3.898 Å. This distance is larger than the one found below for **11**, but still significantly shorter than twice the Rh vdW radius (2.44 Å after Alvarez).[26] In these polymeric structures the anions are located somewhere close to the external zone of the aryls, as shown for the chloride in Figure 3a.

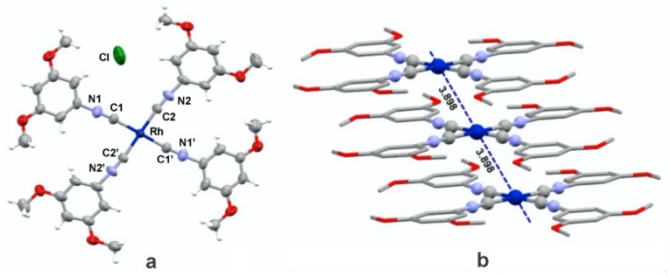

Figure 3. ***a)*** Crystal structure of blue crystals of [Rh(L^C)$_4$](Cl) (**9**). Most prominent distances (Å) and angles: Rh(1)-C(1) = 1.943(9); Rh(1)-C(2) = 1.970(8); C(1)-N(1) = 1.157(11); C(2)-N(2) = 1.134(10); C(1)-Rh(1)-C(2) = 92.8(4); C(2)-Rh(1)-C(3) = 87.2(4); ***b)*** Crystal packaging: infinite chains of [Rh{$CNC_6H_3(OMe)_2$-3,5}$_4$]Cl (**9**), with Rh···Rh = 3.898 Å.

In the case of [Rh(L^A)$_4$](BF$_4$) (**11**), deep red crystals were obtained by slow diffusion of hexane into a diluted solution in acetone of the green solid isolated in the synthesis. A dimeric arrangement of cations, with Rh···Rh = 3.473 Å was found (Figure **4**).

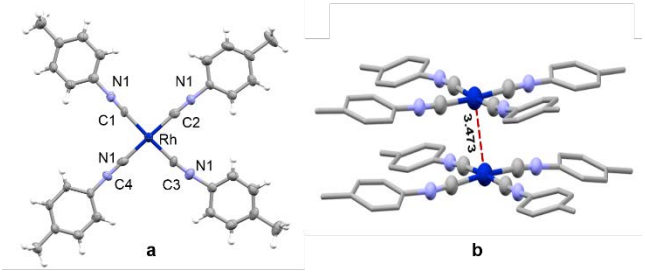

Figure 4. ***a)*** Crystal structure of red crystals of [Rh(L^A)$_4$](BF$_4$). (**11**). BF_4 was omitted to simplify the figure. Most prominent distances (Å) and angles: Rh(1)-C(1) = 1.963(7); Rh(1)-C(2) = 1.967(9); Rh(1)-C(3) = 1.940(8); Rh(1)-C(4) = 1.964(9); C(1)-N(1) = 118(9); C(2)-N(2) = 1.182(10); C(3)-N(3) = 1.147(10); C(4)-N(4) = 1.166(10); C(1)-Rh(1)-C(2) = 91.0(3); C(2)-Rh(1)-C(3) = 86.4(3); C(3)-Rh(1)-C(4) = 92.8(3); C(4)-Rh(1)-C(1) = 89.6(3); C(1)-Rh(1)-C(3) = 174.4(3); C(2)-Rh(1)-C(4) = 177.3(3); ***b)*** Crystalline packaging: dimers of [Rh(L^A)$_4$](BF$_4$).

The deep colours of the blue crystals of [Rh(L^C)$_4$](Cl) (**9**) and the red crystals of [Rh(L^A)$_4$](BF$_4$) (**11**) are typical of Rh complexes that display π-π stacking interactions inducing Rh^I···Rh^I short distances, as also observed in other similar deeply coloured Rh^I complexes in the literature. These Rh^I oligomers or polymers with Rh^I···Rh^I interactions can display colours in the red-to-blue range. The π-π stacking, Rh···Rh distances and aryl substituents are interconnected properties. For instance, **11**, a dimer with good π-π stacking (short Rh···Rh distance = 3.473 Å) is red, but the analogous dimers [Rh_2{(*p*-$CNC_6H_4F)_4$}$_2$]Cl_2·$(OH_2)_2$ (Rh···Rh = 3.207 Å and [Rh_2{(*p*-$CNC_6H_4(NO_2))_4$}$_2$]Cl_2 (Rh···Rh = 3.25 Å are blue and deep green, respectively.[1e] Clearly, in this case the colour switch is due to the change of *p*-substituent (Me gives red but the electron withdrawing F and NO_2 substituents give green-blue). The structurally different crystals of the polymeric complex **9**, with 3,5-OMe substituents and a less efficient packing (Rh···Rh = 3.898 Å) are also deep blue. Note also that polymers, having the aryl π electron density involved in double π-π stacking, lead to longer Rh···Rh distances than the dimers. For electronically similar substituents (H, Me) the colour could be expected to be mainly a function of the structure, that is, of the efficiency of the stacking and, consequently, of the Rh···Rh distances. Y. Yamamoto *et al.* estimated the different spatial requirements of some 2,6-substituents in rhodium complexes of 2,6-disubstituted

phenyl isocyanides,[1d] by means of values of the "wideness angle" and the "thickness angle", defined by the tangents from the Rh atom centre to the atoms marking the molecular frontiers of the substituted aryls in the plane and in the C_{ipso} direction. These angles are 77º and 48º for PhNC versus 106º and 53º for 2,6-Me-C_6H_4NC from Rh. The bulkiness of the isocyanides, as estimated by these angles, can impose the necessity for the isocyanide aryls to adopt smaller or larger twists relative to the RhC_4 coordination plane. Small twists will be compatible with good π-π stacking and short Rh···Rh distances in dimers. Large twists weaken the strength of the π-π stacking and bring to longer Rh···Rh distances compatible with polymeric structures or, in the limit, to formation of monomers, as in the case of the yellow complex $[Rh(CNXylyl)_4](BF_4)$,[10] whose X-ray diffraction structure consists of monomeric cation units, with no π-π stacking and no Rh···Rh interactions.

Our main interest in this work is centred on the triphenylene isocyanide complexes with **L^{D1}** or **L^{D2}** (Scheme 2: **10**, **14**, **15**, **19**, **20**). Not unexpectedly, due to the presence of long alkoxylic chains, it was impossible to obtain single crystals of any of them but their solid state or mesomorphic structures (see later) should be conditioned by the two moieties prone to columnar π-π stacking: the TPh triphenylene (TPh) groups and the aryls of the $[RhL_4]$ groups. Concerning the latter, the 2,6-Me substituted **L^{D2}** complexes should give less efficient π-π stacking than those with **L^{D1}**. This difference can occasionally produce significant differences in their properties, whether in concentrated solution, in the mesophase or in the solid state.

Considering the fairly similar electronegativity of the 2,6- aryl substituents of **L^{D1}** or **L^{D2}** (H and Me, respectively), it is not unreasonable to take the colours of their analogous complexes as indicative of their structures. The pristine solids of three complexes with **L^{D1}** (Cl^-, BF_4^- or $[Au(CN)_2]^-$ as anion), obtained by crystallization, are deep green, and the two complexes with ligand **L^{D2}** (BF_4^- or $[Au(CN)_2]^-$ as anion) are orange-red-brownish solids. This difference in colour is clearly produced by the change of ligand and has nothing to do with the absence or presence of $[Au(CN)_2]^-$ as anion. While the green colour of the complexes with **L^{D1}** is typical of polymeric Rh···Rh interactions (as in **9**), the orange-red colour of the **L^{D2}** complexes might suggest that the two Me substituents in the arylisocyanide moiety hamper a polymeric π-π stacking of $[Rh(CNAr)_4]^+$ cations, perhaps in favour of dimers (as in **11**). This is just a tentative interpretation at the moment, but it finds some support later on.

Photophysical and electrochemical behaviour in solution

The triphenyleneisocyanide-containing complexes show very weak luminescence in solution, which was not further studied.[2,3b,2730] The UV-vis absorption spectra of the new ligand **L^{D2}** (**L^{D1}** was reported in reference 23b) and the complexes **7-20** (Scheme 2) were recorded for 10^{-5} M and 5×10^{-5} M solutions in CH_2Cl_2. The data are collected in Table ESI3 and in Figures ESI36-SI41. They all show intense bands below 400 nm that, according to the literature,[3a] are associated to intraligand $4dz^2(Rh)\rightarrow5p$ transitions. Bands around 450 nm only appear at high concentrations, indicating that they are associated to 4dσ(Rh2)→5pσ(Rh2)/(isocyanide) HOMO/LUMO charge transfer transitions in rhodium dimers.

For the complexes with triphenyleneisocyanides, a band at 280 nm typically associated to the triphenylene group is additionally observed, with the usual extinction coefficients for triphenylene chromophores.[23] The UV-Visible spectra in Figure 5, are representative of the complexes with the triphenyleneisocyanide ligands **L^{D1}** or **L^{D2}**. They are very informative about the formation of Rh···Rh interactions in CH_2Cl_2 solution. All the spectra display a broad and intense absorption. This absorption dominates the spectrum in the more diluted solutions, where the Rh complexes are monomeric, and contains the intraligand transitions for arylisocyanide complexes mentioned above, plus those due to the triphenylene groups. Weak bands supporting Rh···Rh interactions, about 465 nm in the case represented in Figure 5, can be additionally detected only for the higher concentrations (10^{-4}-10^{-3}M). Since the spectra are identical for complexes with $(BF_4)^-$ or $[Au(CN)_2]^-$ as anion, and for **L^{D1}** or **L^{D2}** as ligand, the formation of Rh···Au interactions in "concentrated" (10^{-3} M) solutions can be excluded: the formation of oligomers and the associated colors is due to $L_4Rh\cdots RhL_4$ interactions. This is in coincidence with our previous study, where Rh···Au interactions where only formed in the solid state.[10]

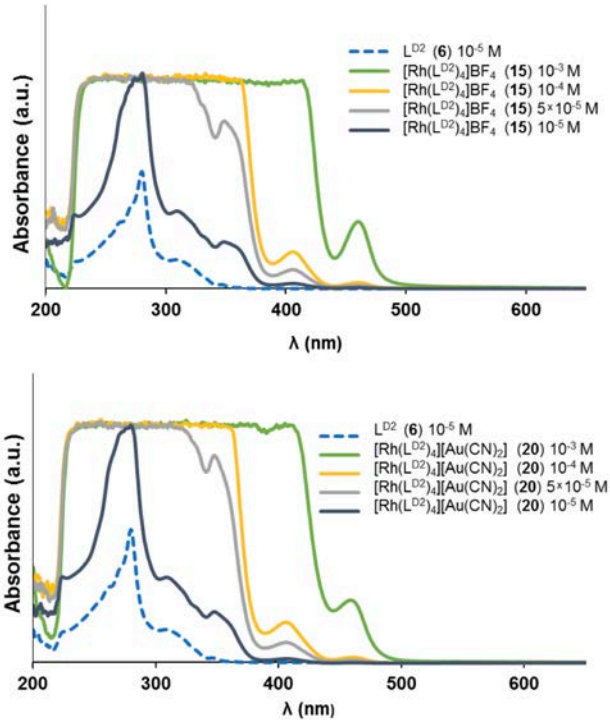

Figure 5. UV-vis spectra of complexes of $[Rh(L^{D2})_4](BF_4)$ and $[Rh(L^{D2})_4][Au(CN)_2]$ at different concentrations.

Additional support that Rh···Rh association in solution not only occurs in the complexes with small substituents at the isocyanide aryl but also for the triphenyleneisocyanide complexes, comes from electrochemical studies. Cyclic voltammetry studies were performed for ligands **L^{D1}** and **L^{D2}**, for complexes **10**, **14**, **19** (with **L^{D1}**), and for complexes **15** and **20** (with **L^{D2}**). The cyclic voltammetry measurements were carried out on dilute (5×10^{-5}M) and concentrated (10^{-3}M) solutions of the complexes CH_2Cl_2 solutions with tetra-n-butylammonium hexafluorophosphate (0.1 M) and the. Complete data of electrochemical parameters and HOMO/LUMO Energy Levels in Table ESI4 and in Figures ESI62-SI63.

All the compounds, except the ligands **L^{D1}** and **L^{D2}** and complex **10** (10^{-3}M), show irreversible oxidation processes. In dilute solutions the complexes give an intense peak in the range 0.89–1.05 eV. This oxidation peak appears also in the solutions of both ligands and therefore it corresponds to the energy of the HOMO orbital for the triphenylene system.[31] Additionally, a second oxidation peak, in the range 1.27–1.60 eV, appears only in the concentrated solutions of the complexes. Since this oxidation peak is always observed,

independent of the anion, it is assigned to the HOMO energy of the oligomeric $Rh^{I}\cdots Rh^{I}$ species in solution. The case of $[Rh(\mathbf{L^{D1}})_4][Au(CN)_2]$ (Figure 6) is representative of this general behaviour and shows how the reversible voltammogram of the monomeric complex at the lower concentration is intruded at higher concentration by the participation of oligomeric species with Rh···Rh interactions, as detected in the UV-vis spectra (Figure 5).

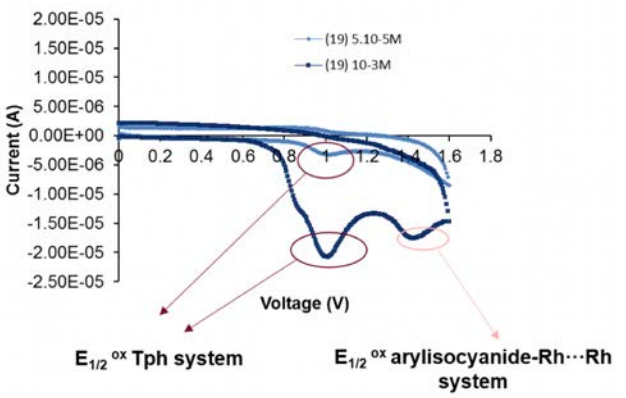

Figure 6. Cyclic voltammogram of $[Rh(L^{D1})_4][Au(CN)_2]$ in CH_2Cl_2 at two molar concentrations.

Overall, the photophysical and cyclic voltammetry data in CH_2Cl_2 solution confirm the molecular association and formation of Rh···Rh interactions the Rh complexes studied, at molar concentrations above 10^{-4}. Moreover, they also support the absence of Rh···Au interactions in solution when $[Au(CN)_2]^-$ is used as counteranion.

Thermal and mesomorphic behavior

The mesomorphic properties have been studied with polarized optical microscopy (POM), differential scanning calorimetry (DSC), small- and wide-angle X-ray scattering (S/WAXS), and grazing incident WAXS (GIWAXS).

The mesophases obtained are very viscous and their transitions occur slowly (in fact the DSC studies show transition curves spanning up to 20-30 °C at the base) with large coexistence of the two mesophases involved in the transition (Figure 7).

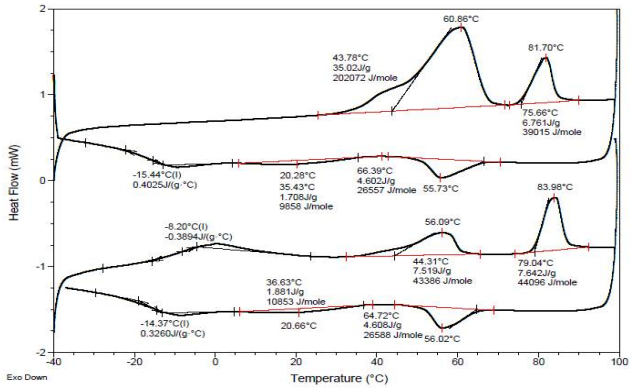

Figure 7. First and second heating/cooling cycles for $[Rh(L^{D2})_4](BF_4)$ (**15**).

Thermal and thermodynamic data are gathered in Table 3 and geometrical data of the mesophases are collected later in Table 4. Neither $\mathbf{L^{D1}}$ nor L^{D2} are mesomorphic, but a rich mesomorphism was induced in their Rh^{I} complexes (Table 3), which display good thermal stability in the range of study. The data in Table 3 correspond to the second heating. Upon cooling after the first heating, compounds **14**, **15**, **19** and **20** do not revert to the crystalline phase obtained from the solution, but to a glass phase. For this reason their second heating start at lower temperatures and generate mesophases below 0 °C, roughly reproducing the first cooling cycle.

Table 3: Thermal and thermodynamic data of $[Rh(L^{D1})_4](A)$ and $[Rh(L^{D2})_4](A)$ complexes (phase transition temperatures, ΔC_p, and ΔH).

Comp.	Transition[a]	T °C[b]	ΔC_p[b] (J/g °C)	ΔH[b] (kJ/mol)
$\mathbf{L^{D1}}$ **(ref. 23b)**	Cr→ I	49		81.6
L^{D2}, **6**	Cr → Cr_2	46.3	-	56.54
	Cr_2→ Cr_3	52.7	-	5.08
	Cr_3→ I	58.5	-	2.12
$[Rh(L^{D1})_4](A)$				
10 A = Cl	Cr→ $Col_{o/r}$[c]	-3.3	-	93.15
	$Col_{o/r}$[c]→Col_r	49.5	-	1.46
	Col_r→I	91.7	-	18.86
14 A = BF_4	g→ $Col_{o/r}$[c]	-9.4	0.70	-
	$Col_{o/r}$[c]→Orth	137.5	-	1.15
	Orth →I	154.2	-	15.83
19 A = $[Au(CN)_2]$	g→ $Col_{o/r}$[c]	-7.9	0.25	-
	Col_{r1}→Col_{r2}	34.0	-	46.05
	Col_{r2}→I	169.2	-	32.50
$[Rh(L^{D2})_4](A)$				
15 A = BF_4	g→ Amo_{Col}	-8.20	0.39	-
	Amo_{Col} →Col_o	44.3[d]	-	43.39
	Col_o →I	79.0	-	44.10
20 A = $[Au(CN)_2]$	g→ Amo_{Col}	-5.0	0.35	-
	Amo_{Col}→ Col_o	48.0	-	26.53
	Col_o →I	89.7[d]	-	49.18

[a]Cr, Cr_1, Cr_2, Cr_3: Crystalline and poorly developed crystalline phases; g: glass, Amo_{Col}: Amorphous superlattice-like order in the solid state with local-range oblique symmetry; Col_r (Col_{r1} and Col_{r2}): Rectangular columnar mesophase; Col_o: Oblique columnar mesophase; Orth: Orthorhombic mesophase; I: Isotropic Liquid. [b]Data from second heating (transition onset temperatures). Heating and cooling at 10 °C/min. Ovl. = overlapped. [c]Col_o at 20 °C from thin-film and Col_r at 20 °C from bulk. [d] Overlapped.

The samples need to be pressed and sheared frequently under the cover glass during the POM studies in order to help for formation of homogeneous samples against the inertia retarding the phase transitions. Even with this caution, the transition temperatures are submitted to significant uncertainty. The heating/cooling evolution of the materials is clearly seen in Figure 8 for complex **15**.

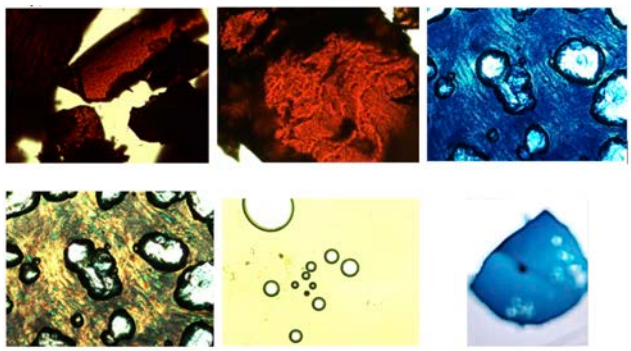

Figure 8. First heating/cooling cycle for $[Rh(L^{D2})_4](BF_4)$ (**15**), as seen without polarizers for better colour observation.

This complex is red-orange in the solid (up-left, 20 °C) and, upon melting (up-centre, 30 °C) changes slowly to a deep blue mesophase (up-right, 70 °C); at the clearing point it starts to be more fluid and, with evanescent green microdomains appearing (down-left, 80 °C), eventually melts to a light yellow isotropic liquid (down-centre, 95 °C). The blue colour is recovered upon cooling to give finally a blue glass phase (down-right is the studied sample in the glass support at 20 °C). The initial red is never thermally recovered.

A very remarkable observation of different behaviour between complexes [(Rh(**L^{D1}**)$_4$](A) and [(Rh(**L^{D2}**)$_4$](A) (A = BF_4, [Au(CN)$_2$]) is the huge difference in mesophase range and clearing point of homologous complexes with **L^{D1}** vs. **L^{D2}** (Table 3, compound **14** vs. **19** and **15** vs. **20**), produced by a change apparently small with respect to the whole molecule of the 2-6-substituents in the arylisocyanide moiety. The clearing points of the **L^{D1}** complexes (154.2 for **14** and 169.2 °C for **19** are ca. 70°C higher than for the analogous **L^{D2}** complexes (79.0 °C for **15** and 89.7 °C for **20**). Again, the 2,6-dimetyl aryl substitution in the isocyanide moiety that disturbed the Rh···Rh in the solid state and propitiated the formation of Rh···Au interactions in our previous paper with Xylyl isocyanide,[10] the one that also produces different colours (red) in the pristine solids of **15** and **20** (orange-red) compared to **14** and **19** (green) in this paper, leads to another very distinct effect, this time on the mesophases. Although it is in principle reasonable to think that the columnar interactions between TPh disks is a strong support of the segregated triphenylene and Rh^{I}···Rh^{I} columnar mesophases reported in this work, the melting points reveal that π-π interactions, stronger with **L^{D1}** or weaker with **L^{D2}**, are in both cases are decisive for the stability of the whole columnar structure. When the π-π interactions are strong (**L^{D1}**), the system can sustain heating to 154.2 and 169.2 °C, but when they are weaker (**L^{D2}**) the whole elaborate scaffolding collapses at 79.0 or 89.7 °C,. In fact, the "clearing points" of the free ligands (non-mesogenic) are 58.5 °C for **L^{D2}** and only 49 °C for **L^{D1}**. Thus, it seems that π-π interactions of the isocyanide aryls (aryl:TPh = 1:1) are the main enthalpic contribution to mesophase stability and it is only the cooperation of the two types of column (TPh:Rh = 4: 1, see below in section S/WAXS and GIWAXS studies)) that allows to compensate the largely unfavourable entropic contribution of this kind of self-association and keeps the columnar arrangement standing. For a discussion and examples on the enthalpy/entropy effects in the formation of columnar mesophases see reference 23d.

S/WAXS and GIWAXS Studies.

S/WAXS studies can provide much information about the self-assembling organization of the different phases but almost none about the existence of Rh···Rh interactions. However, the characteristic colours observed in the mesophases (*e.g.* Figure 8) can be taken as qualitative support of their existence. S/WAXS studies confirm that the five complexes (Table 4) self-organize into multi-segregated structures. As anticipated, distinct self-assembled bundles of organometallic cores between piles of stacked triphenylene mesogens, separated from each other by the aliphatic continuum (chains and spacers), are found. All the data of the mesophases obtained from S/WAXS are summarized in Table 4, and the X-ray patterns are shown in Figures 9, 10 and ESI42-47.

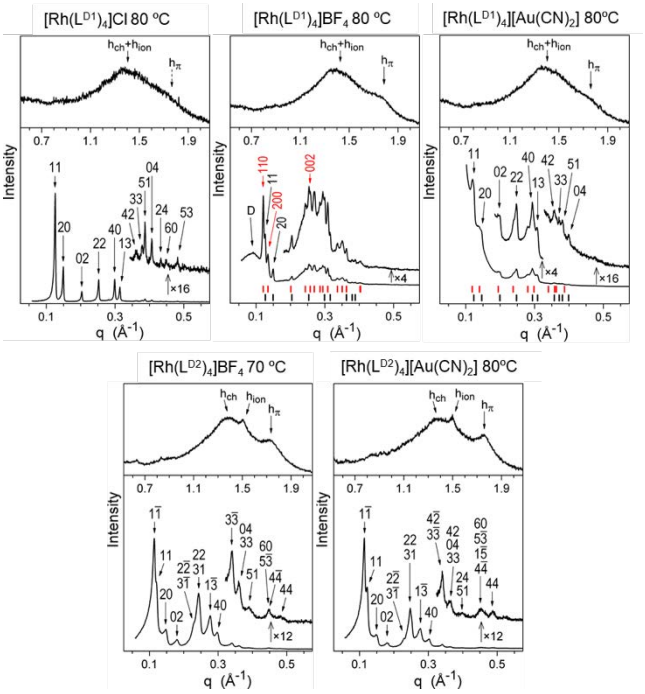

Figure 9. S/WAXS patterns in the fluid mesophase of [Rh(L^{D1})$_4$](A) (Col$_r$ and Orth) and [Rh(L^{D2})$_4$](A) (Col$_o$) at 80°C or 70°C. In red, the signals of the Orth mesophase for the complex [Rh(L^{D1})$_4$](BF$_4$) (14), and the Col$_{r2}$ signals for the complex [Rh(L^{D1})$_4$][Au(CN)$_2$] (19), both coexisting with a Col$_r$ mesophase, whose signals are shown in black.

The presence of only broad signals over the entire X-ray angular domain considered indicates that the pristine solid-state structures are initially only defined at local range, involving few neighbouring molecules. Furthermore, the scattering signature of triphenylene stacking h_π (expected at ca. 3.5 Å) is not separable from scattering contributions of other molecular segments h_{lat}, which indicates irregular pilings. The formation of a superlattice of intermingled domains is however suspected at this early stage by the presence of two intense but broad signals appearing in the small- and mid-angle regions, respectively: a first broad peak, tagged as $D_{Rh/TPh}$, attributed to the average spacing of triphenylenes or organometallic domains separated by chains, and a second, less intense peak, D_{Rh}, from the average spacing of Rh complex domains (Figure ESI43).

On further heating, in concomitance with the increase of the mesophase fluidity, the complexes rearrange into mesomorphic or pre-organized structures, as revealed by the splitting of the broad scattering into two distinct scattering signals, corresponding respectively to the stacking of TPh cores (h_π) and to the packing of chains and ionic moieties (h_{ch}, h_{ion}), and by the evolution of the two former small-angle scattering signals into better-resolved reflection sets, characteristic of the development of a superlattice. This structuring process was not finished for the [Rh(**L^{D1}**)$_4$](A) compounds at the temperature of S/WAXS measurement and required further heating to 120 °C, contrary to [Rh(**L^{D2}**)$_4$](A) compounds already displaying a small-angle region resolved into sharp reflections (Figure ESI46).

ARTICLE

Mesomorphic, Structural, and Geometrical Parameters for complexes $[Rh(L^{Di})_4]A$ (i = 1,2)

A (anion) Sample type / T (°C)[a]	Phase[b]	2D lattice parameters[c] Cell parameters[d]	V_{mol} (Å^3)[e] ρ (g/cm^3) N_{mol},[f]	h_π(Å)[g] h_{mol}(Å)	$Z_{col,RhA}$[h] h_{RhA} (Å) $N_{RhA,c}$	$Z_{col,Tph}$[i] h_{Tph} (Å) $N_{Tph,c}$	⟨ψ$_{Tph}$⟩ (°)[j] $dh_{Tph,c}$ (Å)
$[Rh(L^{D1})_4](A)$							
A = Cl Film / 20	Col_o	*a* = 97(.8); *b* = 53(.3); γ = 97° *A* = 5170 Å^2 (*Z* = 2); *a*/*b* = 1.83	9260 1.00	3.56 3.58	2 3.58	8 3.58	~0
A = Cl Bulk / 20	Col_r	*a* = 84.2(6); *b* = 62.0(7); γ = 90° *A* = 5230 Å^2 (*Z* = 2); *a*/*b* = 1.36	9260 1.00	3.55 3.54	2 3.54	8 3.54	~0
A = Cl Bulk / 80	Col_r	*a* = 84.1(4); *b* = 61.8(4); γ = 90° *A* = 5203 Å^2 (*Z* = 2); *a*/*b* = 1.36	9493 0.98	3.6 3.65	2 3.65	8 3.65	~0
A = BF_4 Film / 20	Col_o	*a* = 98(.5); *b* = 57(.9); γ = 93° *A* = 5695 Å^2 (*Z* = 2); *a*/*b* = 1.70	9282 1.01	3.55 3.26	2 3.26	10 4.07	29
A = BF_4 Bulk / 20	Col_r	*a* = 84.1(2); *b* = 61.8; γ = 90° *A* = 5199 Å^2 (*Z* = 2); *a*/*b* = 1.36	9282 1.01	3.54 3.57	2 3.57	8 3.57	~0
A = BF_4 Bulk / 80	Col_r + Orth	*a* = 83.9(6); *b* = 61.4(9); γ = 90° *A* = 5163 Å^2 (*Z* = 2); *a*/*b* = 1.36 *a* = 93.4; *b* = 62.4(5); γ = 90° *A* = 5833 Å^2 (*Z* = 2); *a*/*b* = 1.50 *c* = 48.4(4); *V* = 282500 Å^2	9515 0.99 9515 0.99 29.7	3.55 3.69 3.55 3.26	2 3.69 2 3.26 14.8	8 3.69 10 4.08 11.9	16 0 5.5
A = BF_4 Bulk / 120	Orth	*a* = 90.8(8); *b* = 63.3; γ = 90° *A* = 5753 Å^2 (*Z* = 2); *a*/*b* = 1.44 *c* = 48.3(7); *V* = 278300 Å^2	9671 0.97 28.8	3.60 3.36	2 3.36 14.4	10 4.20 11.5	0 6.5
A = $Au(CN)_2$ Film / 20	Col_o	*a* = 96(.6); *b* = 55(.0); γ = 96° *A* = 5284 Å^2 (*Z* = 2); *a*/*b* = 1.76	9316 1.00	3.50 3.53	2 3.53	8 3.53	~0
A = $Au(CN)_2$ Bulk / 20	Col_r	*a* = 86.1(5); *b* = 63.2(9 γ = 90° *A* = 5452 Å^2 (*Z* = 2); *a*/*b* = 1.36	9316 1.04	3.54 3.42	2 3.42	undefin ed	undefined
A = $Au(CN)_2$ Bulk / 80	Col_{r1} + Col_{r2}	*a* = 85.5(5); *b* = 62.9(7); γ = 90° *A* = 5387 Å^2 (*Z* = 2); *a*/*b* = 1.36 *a* = 89.8; *b* = 64.9(6); γ = 90° *A* = 5832 Å^2 (*Z* = 2); *a*/*b* = 1.38	9550 1.01 9550 1.01	3.57 3.55 3.57 3.27	2 3.55 2 3.27	8 3.55 10 4.09	~0 29
A = $Au(CN)_2$ Bulk / 120	Col_{r2}	*a* = 88.6(8); *b* = 64.9; γ = 90° *A* = 5755 Å^2 (*Z* = 2); *a*/*b* = 1.37	9706 0.99	3.58 3.37	2 3.37	10 4.22	32
$[Rh(L^{D2})_4](A)$							
A = BF_4 Film / 20	Col_o	*a* = 81(.3); *b* = 60(.9); γ = 96° *A* = 4930 Å^2 (Z = 2); *a*/*b* = 1.33	9492 1.01	3.55 3.85	2 3.85	8 3.85	23
A = BF_4 Bulk / 70	Col_o	*a* = 84.7(7); *b* = 69.5(4); γ = 93.5(8)° *A* = 5883 Å^2 (Z = 2); *a*/*b* = 1.22	9691 0.99	3.60 3.29	2 3.29	10 4.12	29
A = $Au(CN)_2$ Film / 20	Col_o	*a* = 75(.1); *b* = 49(.6); γ = 96° *A* = 3705 Å^2 (Z = 2); *a*/*b* = 1.51	9527 1.03	3.56 5.14	2 5.14	6 3.86	22
A = $Au(CN)_2$ Bulk / 80	Col_o	*a* = 83.7(6); *b* = 69.5(2); γ = 93.9(4)° *A* = 5810 Å^2 (Z = 2); *a*/*b* = 1.21	9767 1.01	3.56 3.36	2 3.36	10 4.20	32

[a]T: temperature of the measurement; [b]Col_o, Col_r, Col_{r1}, Col_{r2}: oblique and rectangular columnar structures; Orth: orthorhombic structure; [c]*a*, *b*, γ, *A* = *a*×*b*×sinγ, *Z*, *a*/*b*: lattice parameters, lattice area, number of molecular elementary motif per lattice and lattice parameter ratio; [d]*c*, *V*: lattice parameter and cell volume of Orth mesophase; [e]V_{mol}, ρ: molecular volume and density; [f]N_{mol}: number of molecules per cell (Orth mesophase); [g]h_π: average distance between stacked triphenylene (TPh) rings from position of scattering maximum in pattern; h_{mol} = (*Z*×V_{mol})/*A*: molecular slice thickness; [h]$Z_{col,RhA}$, h_{RhA} = ($Z_{col,RhA}$/*Z*)×h_{mol}: number of piles per lattice and molecular slice thicknesses for rhodium complexes and counter-ions (RhA); $N_{RhA,c}$ = *c*/h_{RhA}: number of RhA units per pile and unit cell (Orth phase); [i]$Z_{col,Tph}$, h_{Tph} = ($Z_{col,TPh}$/4*Z*)×h_{mol} number of columns per lattice and molecular slice thicknesses for Tph; $N_{Tph,c}$ = *c*/h_{Tph}: number of Tph units per column and unit cell; [j]⟨ψ$_{Tph}$⟩ = acos(h_π/$h_{Tph,col}$): mean out of plane tilt angles of piled Tph units; $dh_{Tph,c}$ = c - $N_{Tph,c}$× h_π: interruption zone thickness of segmented Tph columns (Orth phase). ***For the meaning of "RhA units" and "TPh units" see Figure 11.***

ARTICLE

After annealing the complexes in their high-temperature mesophase or at slightly higher temperatures for 10-15 minutes, temperatures were slowly decreased, and S/WAXS and GIWAXS patterns were recorded at 20 °C in the bulk and in thin films, respectively (Figures ESI45-46). The three compounds of the [Rh(**L^{D1}**)$_4$](A) series display, independently of the anion, a frozen rectangular columnar mesophase (Col$_r$) in the bulk state, characterized by a series of sharp reflections of a large-size two-dimensional rectangular *c*2*mm* lattice (Table 4, with a ≈ 84-86 Å, and b ≈ 62-63 Å) and by the scattering signals from π-π stacking h_π and molten chain packing h_{ch}. In addition, the S/WAXS pattern of [Rh(**L^{D1}**)$_4$](BF$_4$) presents a broad small-angle peak D arising from a local range periodicity, whilst that of [Rh(**L^{D1}**)$_4$][Au(CN)$_2$], a small-angle scattering upturn due to some structural disorder. On the contrary, both [Rh(**L^{D2}**)$_4$](A) compounds lose the long-range order on cooling (see below, and Figure 9) and give amorphous-like states preserving some residual columnar structure correlated over few molecules (short-range ordered oblique lattice Amo$_{Col}$), as revealed by the broadened reflections in the small-angle region and by wide-angle scattering maxima.

The GIWAXS patterns of thin films of all the complexes display well-oriented columnar mesomorphic organizations, with [10] or [11] crystallographic direction aligned onto the film normal (Figure ESI46). Films of [Rh(**L^{D1}**)$_4$](A) also reveal large superlattices developed to long-range as in the bulk state, but the symmetry is lowered to oblique (Col$_o$). As for the bulk, film states of [Rh(**L^{D2}**)$_4$](A) compounds display oblique superlattices (Col$_o$), but the detailed arrangements are different (see below).

Re-heating the samples to 80 °C, the Col$_r$ mesophase formed by the three [Rh(**L^{D1}**)$_4$](A) compounds is identical to the structure frozen in the solid state at 20 °C, and is characterized by a *c*2*mm* superlattice of nearly same size for the three compounds (Figure 9, Table 4). The piling of TPh units is rather irregular, considering the weak h_π signal, hardly distinguishable from the scattering maxima of the molten chains, h_{ch}, and ion packing, h_{ion} (Figure 9, Table 4). Whilst for [Rh(**L^{D1}**)$_4$]Cl, only one phase is present, for both [Rh(**L^{D1}**)$_4$](BF$_4$) and [Rh(**L^{D1}**)$_4$][Au(CN)$_2$], the Col$_r$ mesophase coexists with another mesophase, likely due to some slow re-organization kinetics (Figure 9, signals pointed by red labels and position marks; black labels and marks for Col$_r$). For the complex with the BF_4^- anion, this phase is identified to a three-dimensional orthorhombic mesophase (Orth) and for the other complex with $[Au(CN)_2]^-$, to a second rectangular *c*2*mm* phase of larger lattice area (Col$_{r2}$, Table 4). Both [Rh(**L^{D2}**)$_4$](A) compounds organize into oblique columnar mesophases (Col$_o$) closed to the one formed in thin films (Figure 9). Beyond the lattice symmetry change, patterns differ from corresponding [Rh(**L^{D1}**)$_4$](A) compounds by the absence of short-range periodicity or scattering upturn in the small-angle region, as well as by the wide-angle region well-resolved into individual h_{ch}, h_{ion} and h_π signals, which indicates a regular arrangement with low degree of structural disorder.

The mesophases of [Rh(**L^{D1}**)$_4$](BF$_4$) and [Rh(**L^{D1}**)$_4$][Au(CN)$_2$] were further investigated at higher temperature. At 120 °C, both complexes are still mesomorphic and display the neat orthorhombic and Col$_{r2}$ phases (Figure 10), respectively, and the reverse transition to the low-temperature Col$_r$ phase being in both cases observed on cooling. The a×b sublattice of the Orth phase designs a rectangular *c*2*mm* lattice of dimensions comparable to the Col$_{r2}$ lattice and substantially larger than the low-temperature Col$_r$ lattices. Apart from the appearance of the three-dimensional superstructure, Orth and Col$_{r2}$ differ by the regularity of the TPh piling, since the h_π scattering is blurred out in the 3D phase and on the contrary amplified relatively to Col$_r$ in the 2D phase.

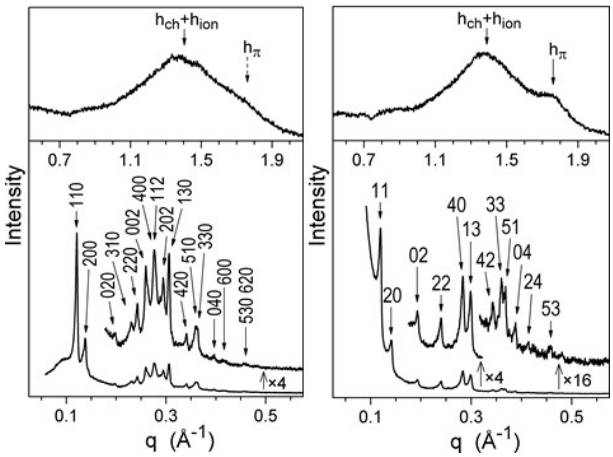

Figure 10. S/WAXS patterns of [Rh(**L^{D1}**)$_4$](BF$_4$) and [Rh(**L^{D1}**)$_4$][Au(CN)$_2$] at 120 °C in the Orth and Col$_{r2}$ mesophases, respectively.

At 120 °C the complexes [Rh(**L^{D1}**)$_4$](Cl), [Rh(**L^{D2}**)$_4$](BF$_4$) and [Rh(**L^{D2}**)$_4$][Au(CN)$_2$] have reached the isotropic liquid state. The eradication of any regular structure is confirmed by the merging of the wide-angle signal into a unique maximum overlapping all lateral distances between molecular segments (h_{lat}, Figure ESI41). Simultaneously, the D_{Rh} and $D_{Rh/TPh}$ scattering peaks from pristine solid states reappear in the small-angle region, meaning that a columnar superlattice-like organization is maintained at the local range between neighbouring molecules.

Discussion of the self-organization behaviour.

Recall that the two experimental X-ray setups used must be distinguished, which result in some differences in the supramolecular self-assembly: (i) the thin-film configuration (GIWAXS), in which the sample in the mesophase is deposited on a silicon wafer by spin-coating at 20 °C to form a very thin film, and (ii) the bulk configuration (S/WAXS), where the material is maintained in a closed cell. This latter corresponds to the usual method of microscopic observation at variable temperatures.

Independently of the configuration used for the measurements, the large 2D lattice parameters of the mesophases (a and b, Table 4) and the distinct S/WAXS signals, corresponding respectively to the metallic fragment and triphenylene parts, confirmed, in agreement with the detailed crystallographic analysis of reference compounds, that both multiblock [Rh(**L^{D1}**)$_4$](A) and [Rh(**L^{D2}**)$_4$](A) complexes self-assemble into multi-segregated columnar structures made of differentiated metal-containing piles and triphenylene columns, respectively. Also, whatever the experimental situation, the

assembly of the metallic fragment part and counter-ion comes down to a platelet-like "RhA" subunit resembling to a “discotic” mesogen with even piling distance (3.53 Å for RhA in $[Rh(CNXylyl)_4](BF_4)$,[10] close to the normal triphenylene stacking periodicity ($h_\pi \approx 3.5$ Å for TPh), but obviously of different chemical nature. In the single-crystal structure of the compound $[Rh(CNXylyl)_4](BF_4)$, analogue to $[Rh(\mathbf{L^{D2}})_4](BF_4)$ without alkoxytriphenylene substituents, the counter-ions locate in the same plane of the metallic centre and both superimpose (with lateral shift and inversion) to complex and counter-ions of the next molecular layer (Figure 11, supramolecular model).

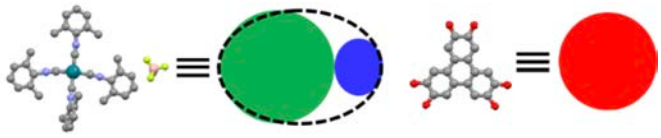

Figure 11. *Left*: schematic graphic representation of $[RhL_4](A)$ units. *Right*: Tph units. The crystal structure of $[Rh(CNXylyl)_4](BF_4)$ is used as real model.[10]

Such structures are effectively obtained throughout both series of complexes with molecular slice thicknesses h_{RhA} (ranging from 3.25 to 3.85 Å, Table 4) indicative of RhA arrangements not far from the reference single-crystal. One notable exception is for $[Rh(\mathbf{L^{D2}})_4][Au(CN)_2]$ in film whose substantially higher h_{RhA} value (5.14 Å) is compatible with the intercalation of complex and counter-ion along columns, as in the single-crystal structure of the $Au(CN)_2^-$ reference complex.[10] Intercalation is on the contrary excluded for $[Rh(\mathbf{L^{D1}})_4][Au(CN)_2]$ (h_{RhA} = 3.53 Å), but both $Au(CN)_2$-containing Rh complexes give fluid mesophases at higher temperatures with even lower h_{RhA} values (3.3 – 3.4 Å). This evolution probably signifies that the intercalated configuration is optimal for the simple ionic systems but that the juxtaposed configuration prevails as it enables a more compact packing of the bulky substituents. Regarding the Tph units, h_π and h_{mol} values are mostly in agreement with those of the solid state, indicating that molecules merely pile into molecular stacks and form the columnar superlattices by intermingling their Tph columns. As for the arrangements of the two types of columns within the large 2D lattices, let us first examine the thin film situation, at room temperature. In this case, all the compounds form oblique columnar structures (Table 4), made of two types of molecular piles per lattice: the Rh complexes and counter-ions superimposed into "RhA" columns (green) occupying the centre of a honeycomb-like sublattice of "TPh" columns (red) separated by molten chains (Figure 12, chains not represented). In the $[Rh(\mathbf{L^{D1}})_4](A)$ series and in $[Rh(\mathbf{L^{D2}})_4](BF_4)$, counter-ions are located in the periphery of piled complexes and essentially contribute to the cross-sectional area of the columns, piling distances of Rh complexes and TPh being similar. The formation of a compact honeycomb thereby requires 8 neighbouring TPh columns with Cl and $[Au(CN)_2]$ anions, in agreement with the 1:4 molecular stoichiometry. With BF_4, TPh shares between 10 neighbouring columns, which corollary implies out-of-plane tilting of rings to compensate for their higher intracolumnar spacing. With the more voluminous $\mathbf{L^{D2}}$ ligand, compactness is achieved for the BF_4 complex with 8 neighbouring columns and tilting of both, RhA and TPh. For the $\mathbf{L^{D2}}$ and $Au(CN)_2$ pair (see later), anion and complex intercalate to elongated RhA columns, which is counterbalanced by the reduction of neighbouring TPh to 6 tilted columns.

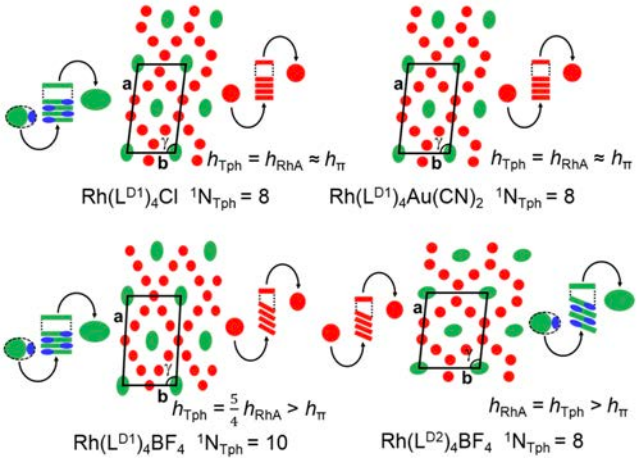

Figure 12. Schematic views of the supramolecular organizations of $[Rh(\mathbf{L^{D1}})_4](A)$ ($A = Cl^-, BF_4^-, Au(CN)_2^-$) and $[Rh(\mathbf{L^{D2}})_4](BF_4)$ complexes in oblique multicolumnar mesophases (thin film states).

In different circumstances both stacks may occur inclined in which case the h_{TPh} or h_{RhA} value is different from horizontal stacking. From the variation of these parameters observed in the SWAXS and GIWAXS studies, the distance between disks in the mesophase and their inclination to the horizontal arrangement can be deduced (Table 4).

Figure 12 shows the distribution of TPh columns and RhA columns vertically viewed in the columnar arrangement and should be understood as not assuming a 1:1 ratio between discs because depending on their inclination or not, the distances between discs in a column are not the same. Therefore, while the number N_{TPh} defines the number of columns of TPh per unit cell, in which is contained a column RhA in the centre, and one in each vertex, the ratio of triphenylenes to RhA units must be 4 to 1. Both are related by the different h_{TPh} and h_{RhA} values depending on their inclination.

So, in horizontal stacks in both columns the value of N_{TPh} is 8 and it is met that $h_{TPh} = h_{RhA} \approx 3.5$ Å. This occurs for $[Rh(\mathbf{L^{D1}})_4](Cl)$ (**10**) and $[Rh(\mathbf{L^{D1}})_4][Au(CN)_2]$ (**19**). Obviously, the ratio of red to green columns (8/2 = 4) coincides with the ratio of disks. For $[Rh(\mathbf{L^{D1}})_4](BF_4)$ (**14**) N_{TPh} = 10 because the disks of the TPh columns are inclined, the colours only represent the number of columns but not the number of disks as they are separated differently in the green columns and in the red ones. To reach the obligatory ratio of 4 to 1 to which we have alluded, it is necessary that $h_{TPh} = 5/4\ h_{RhA} > h_\pi$.

For the more voluminous $\mathbf{L^{D2}}$ ligand with BF_4 (**15**), both inclined disk stacks are produced with similar inclination with $h_{RhA} = h_{TPh} > h_\pi$ and 8 adjacent TPh columns around a unit of RhA. Such structures are effectively obtained throughout the series with molecular slice thicknesses h_{RhA} (ranging from 3.25 to 3.85 Å) indicative of RhA arrangements not far from the reference single-crystal (Figure 12 bottom, right).

As hoped for the combination $\mathbf{L^{D2}}$ and $Au(CN)_2$ as anion, Figure 13) shows the interesting exception of complex $[Rh(\mathbf{L^{D2}})_4][Au(CN)_2]$ (**20**), in which h_{RhA} = 5.14 Å is found. This is interpreted as the result of an intercalation of the fragment $Au(CN)_2$ between the disks of the fragment $[Rh(\mathbf{L^{D2}})]$, as depicted in the Figure 13 left. So, RhA has now another nature, because the $Au(CN)_2$ units (blue spots) are not coplanar with the $[Rh(\mathbf{L^{D2}})]$ units (green circles) but pile up intercalating laterally between rhodium disks. As a consequence, the thickness needed to house one gold plus one rhodium is greater and $h_{RhA} = 4/3h_{TPh} >> h_\pi$, which produces 6 TPh columns tilted around RhA. The proposal for the RhA green+blue column (Figure 13, right)

can be compared with the crystalline structure observed for the blue polymorph of [{L_4Rh}{$Au(CN)_2$}{RhL_4}]($Au(CN)_2$) (Figure 13, right). In the mesophase the value h_{RhA} = 5.14 Å excludes a linear Rh···Au···Rh···Au chain as in the crystal, which requires still larger distances between the [Rh(**L^{D2}**)]$^+$ units, but is compatible with a rearranged distribution of the Rh centres along the column, with the intrusion of the $Au(CN)_2^-$ fragments in between successive Rh disks, as depicted schematically in Figure 13, left. This distortion produces a pseudo-zig-zag (--Rh----Au----Rh----Au--)$_\infty$ chain. The "Rh-----Rh" sequence could still keep roughly parallel to the column axis, while the Au atoms take randomly helicoidal positions around this Rh-----Rh axis. Note that this hypothesis on the arrangement of the metal atoms (which are not observable) in the columns is merely proposed on the basis of geometrical constraints and does not presume anything about the potential presence or lack of Rh···Au intermetallic interactions. Electrostatic or dipolar Rh/Cl interactions could also provide the attractions needed to compensate the loss of π-π stabilization in the green columns of Figure 13, left.

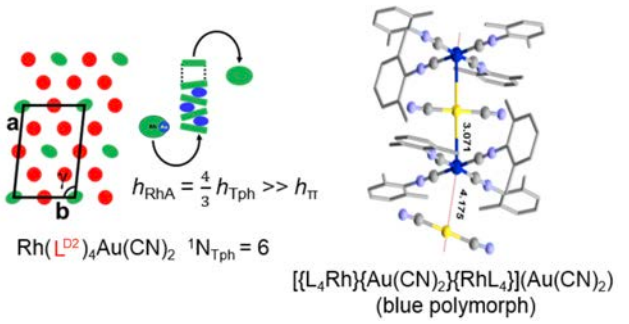

Figure 13. *Left*) Proposed schematic model of molecular self-assembly for complex **20** in thin film sat 20 . *Right*) Crystal structure of complex [{L_4Rh}{$Au(CN)_2$}{RhL_4}]($Au(CN)_2$) (blue polymorph). A zig-zag distorted (--Rh----Au----Rh----Au--)$_\infty$ structure can be imagined from there, as represented in the schematically in the model at left.

In summary, the two complexes containing the dicyanoaurate anion reveal different structural organization within the metallic columns. For **19** (L = **L^{D1}**), the formation of Rh···Rh···Rh stacking is always found. However, for **20** (L = **L^{D2}**), an exception is found (only in thin film mesophase at 20 °C): the 2,6-dimethyl substituents in the arylisocyanide weaken the strength of the π-π stacking, and bring to longer Rh···Rh distances,[1d] which facilitates the lateral intercalation of the anion $Au(CN)_2^-$ in the Rh···Rh stacking to produce a pseudo-zig-zag Rh…Au…Rh chain.

The practically coplanar arrangement of the four aromatic rings in complex **7** allows for a good stacking between units. Specifically, these are arranged as dimers, with a Rh-Rh distance of 3.473 Å (Figure 3b), less than the sum of van der Waals radii, so that both π-π stacks and Rh^I···Rh^I interactions are taking place. This structure is analogous to the dimer [Rh($CNC_6H_4F)_4$](Cl)(OH_2),[1e] in which π-π stacking and Rh^I···Rh^I interactions are observed. In both cases the aryl groups are arranged almost coplanar to the square plane of the metal centre of Rh^I.

The proximity between monometallic units observed in the single crystal structures of complexes **7** and **9** was not found in the previously studied [Rh(CNXylyl)$_4$](BF_4) complex,[10] whose yellow crystals are composed of monomeric units as a result of the lack of coplanarity of their four aromatic rings and Rh···Rh interactions. Therefore, it seems that the Rh···Rh metallic interactions, (or Rh···Au interactions in reference 10, and in one mesophase here) determine the deep blue or green colours of the complexes, while it is the π-π stacking or electrostatic attractions the ones that energetically determine the metal centre approximation that gives rise to formation of metal···metal interactions.

In the solid state, all [Rh(**L^{D1}**)$_4$](A) compounds show a frozen rectangular columnar mesophase **Col$_{r1}$**, with 8 neighbouring TPh columns around RhA, in consistency with the molecular stoichiometry (Figure 14). At higher temperature, the Cl complex early flows to an isotropic liquid state with residual superlattice order, while the molecular organizations of the BF_4 and $Au(CN)_2$ congeners however rearrange in another fluid mesophases with substantially increased superlattice area and lowered h_{mol}, which reveals redistribution of TPh rings with creation of supplementary columns. This process implies that the TPh units are more spaced within columns (larger spacing) and thus introduces a discrepancy with h_π which needs to be compensated either by out-of-plane tilting of rings ($\langle\Psi_{TPh}\rangle > 0$) or by disruption of the columns into segments separated by aliphatic zones ($dh_{TPh,c} > 0$), as previously reported for architectures with single discotic mesogen and overcrowded aliphatic crown.[30] The lattice expansion of the **Col$_{r2}$** phase therefore involves the tilting mechanism, while the **Orth** phase emerges from the 3 dimensional arrangement of segmented columns. The reason of these structural changes is primarily that the fluidizing of the sample at higher temperature effectively enables the redistribution of TPh rings, and presumably that RhA can be compactly surrounded by 10 columns, contrarily to the 8 columns directly obtained from the molecular stoichiometry.

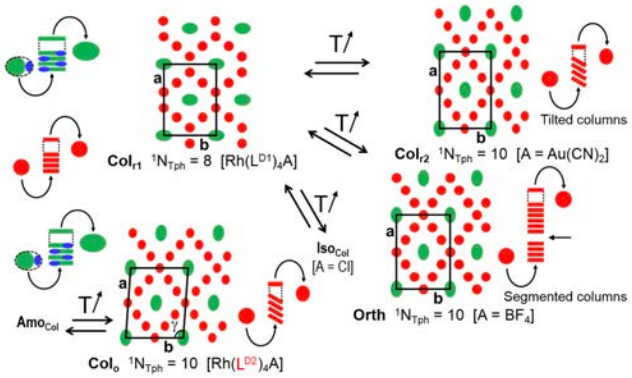

Figure 14. Schematic views of the molecular self-assembling in the bulk states. All compounds form columnar mesophases with superlattice structures based on RhA columns (green) surrounded by honeycomb-like lattices of Tph columns (red) and spaced by molten chains (not represented); the displayed in-plane orientations are in perfect agreement with the phase symmetry and the optimal space-filling, but are otherwise arbitrary.

[Rh(**L^{D2}**)$_4$](BF_4) and [Rh(**L^{D2}**)$_4$][$Au(CN)_2$] show an amorphous undefined superlattice-like order with a local oblique symmetry in the solid state (Amo$_{Col}$). However, both compounds rearrange at higher temperature into fluid oblique columnar mesophases (Col$_o$) with superlattices of large area corresponding to 10 tilted TPh columns. The fundamental variation is that the stacking Rh-Au observed for compound **20** in the film situation, is no longer observed in this bulk situation.

Hole mobility studies

The HOMO energy levels of the complexes determined in the voltamperometric studies are suitable for charge injection from gold electrodes, which opens the possibility for the experimental hole

mobility study of compounds **10**, **14**, **19**, **15** and **20**. Hole mobilities were measured using the Space Charge Limited Current (SCLC) method, on samples approximately 10 μm thick. The details of sample preparation and measurements can be found in the ESI.

SCLC mobility reflects the average mobility across the entire thickness of the sample. In anisotropic media, such as in columnar mesophases, it will significantly depend on the alignment of the columns: it will be higher the more uniformly and macroscopically oriented the columns are along the direction of displacement of the charges. Usually, however, the columnar units do not spontaneously align in the direction of the applied electric field, so it is necessary to use thermal treatments, or other means, to induce the preferred alignment. In the case of complexes **10**, **14**, **19**, **15** and **20** POM showed, before any thermal treatment, an uneven distribution of the mesophase director and, consequently, mobility values in the order of 10^{-8}–10^{-9} $cm^2\ V^{-1}\ s^{-1}$ were measured for all complexes. After the thermal treatments described in the ESI, although a clear change in the orientation of the columns was not observed by POM, in some areas of most samples it was possible to measure a much higher charge mobility. This may be due to the fact that, although the thermal treatment failed to induce a dominant favourable homogeneous orientation throughout the samples, this orientation was still achieved in some areas. Results of the measurements are shown in Figure 15.

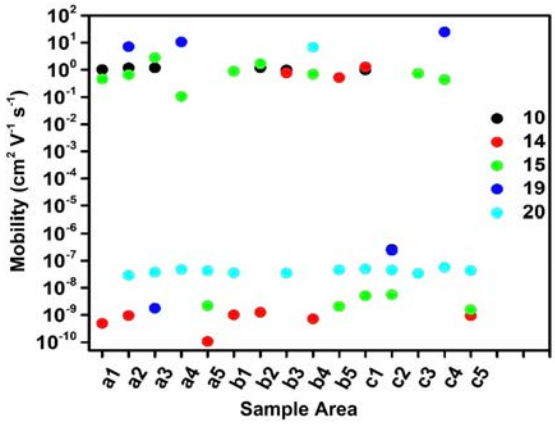

Figure 15. Hole mobilities measured, after thermal treatment, in compounds **10**, **14**, **19**, **15** and **20**. Different areas of each sample are labelled with letters and numbers, as described in the SI.

This "binary" distribution of the measured mobility values after thermal treatments, where the two ranges of measured mobility are separated by 7-9 orders of magnitude, was observed for all samples of all complexes. No intermediate value of mobility was ever recorded. Attributing the very low mobility measured in some sample areas to poor or unfavourable orientation order, such measurements were neglected and charge mobility for each complex was obtained by averaging only the values within the high mobility range. These average results are listed in Table 5.

Table 5. Average measured for hole mobility ($cm^2\ V^{-1}\ s^{-1}$).

Complex	Mobility
$[Rh(\mathbf{L^{D1}})_4](Cl)$ (**10**)	1 ± 0.4
$[Rh(\mathbf{L^{D1}})_4](BF_4)$ (**14**)	0.9 ± 0.6
$[Rh(\mathbf{L^{D1}})_4][Au(CN)_2]$ (**19**)	14 ± 0.5
$[Rh(\mathbf{L^{D2}})_4](BF_4)$ (**15**)	0,9 ± 0.7
$[Rh(\mathbf{L^{D2}})_4][Au(CN)_2]$ (**20**)	8 ± 0.1*

*This datum refers to a single sample area.

It should be remarked that experimental values of charge mobility often depend on the measurement technique and experimental conditions. As a consequence, the values reported in Table 5 should be considered as an order of magnitude estimation rather than as a precise measurement.[32] Yet, since the same experimental conditions were always used, comparison among the results for the five semiconductor complexes is possible.

From the values reported in Table 5, it can be noted that the columnar mesophases of this study show a much higher charge mobility than the values recorded and reported in mesophases formed by triphenylene columns only, usually in the 10^{-4} – 10^{-2} $cm^2\ V^{-1}\ s^{-1}$ range.[15] This indicates that columns formed by the metal-anion pair play a very important role in determining the charge mobility values of the studied complexes. The same behaviour was reported also in mesophases formed by triphenylene-metal complexes with respect to mesophases formed by triphenylene only, both in the case in which the triphenylene columns are segregated with respect to the columns formed by the metal,[23d,23f] and in the case in which they are not.[33] It is also possible to note a dependence of charge mobility on the nature of the anion: with $[Au(CN)_2]^-$ the mobility is one order of magnitude higher than with $(BF_4)^-$ or Cl^-. Since this occurs for the complexes with both $\mathbf{L^{D1}}$ and $\mathbf{L^{D2}}$ and since the strict conditions under which Rh-Au intercalation occurs probably exclude its presence in the samples used for the measurement of hole mobility, this phenomenon is more likely associated to the presence of columns of the ionic pairs $[Rh(\mathbf{L^{D1}})_4](Au(CN)_2)$ or $[Rh(\mathbf{L^{D2}})_4](Au(CN)_2)$ non-intercalated, as shown in Figure 12. Some contribution of Au···Au interactions of the $[Au(CN)_2]^-$ anions in these discotic $[RhL_4][Au(CN)_2]$ might explain this extra hole mobility, but we cannot provide any experimental support for this hypothesis.

Conclusions

Two families of mesogenic complexes with triphenyleneisocyanides, $[Rh(\mathbf{L})_4](A)$ (L = $\mathbf{L^{D1}}$ or $\mathbf{L^{D2}}$; A^- = Cl^-, $(BF_4)^-$ or $Au(CN)_2^-$) have been prepared and their properties studied. All members of both families generate mesophases with multicolumnar structures containing two types of columns: those formed by π-π stacking of triphenylenes, and those resulting from π-π stacking of the organometallic $[Rh^I(ArNC)_4]^+$ units, both being connected by a hexamethylene spacer. Several 2D mesophases with different symmetries and columnar arrangements (Col_r, Col_o) and a 3D mesophase (Orth) are observed in these unique molecular systems. The structural features of the mesophases are conditioned by the isocyanide substituents, the type of anion used, and the conditions and temperature of the experiments carried out. These conditions result in compensating inclinations between the TPh disks and the RhA units that drive and define the network symmetry found in the mesophases.

For the ligand $\mathbf{L^{D1}}$, with no or small tilting of the aryls relative to the RhC_4 square plane, the four isocyanide ligands can strongly cooperate in the intra-unit π-π stacking, thus overcoming the cation-cation repulsions and giving rise to polymeric column formation with Rh···Rh interactions. These interactions lead to mesophases with deep green colours and large mesogenic intervals (from –9 to 169 °C).

The presence of two *ortho*-substituents in the aryl of $\mathbf{L^{D2}}$, which force larger tilting of the aryls that hampers achieving the best π-π aryl stacking, the blue colours and the similarity in columnar parameters with the $\mathbf{L^{D1}}$ complexes still support polymeric Rh···Rh interactions with clearly shorter but still large mesogenic intervals (from –8 to 89 °C). There is only one exception to this structural behaviour in the

mesophases of the complexes with L^{D2}: with $[Au(CN)_2]^-$ as counter-anion, and only in thin films at 20 °C, the substantially higher value of h_{RhA} (5.14 Å, compared to a 3.4-3.55 Å range for the rest of the mesophases) is compatible with the intercalation of the Rh cationic complex and the Au counter-ion along columns to give zig-zag Rh···Au···Rh···Au helicoidal atomic arrangement with anion-cation attractions compensating the loss of the relatively inefficient π-π aryl stacking, as found previously in the related single-crystal structure of the reference complex $[\{L_4Rh\}\{Au(CN)_2\}\{RhL_4\}](Au(CN)_2)$ (blue polymorph).[10] This produces elongated RhA columns, which is counterbalanced by the reduction of neighbouring TPh to 6 tilted columns. The structurally singular zig-zag Rh----Au----Rh----Au organization in this mesophase with L^{D2} does not prevail at higher temperatures and evolves to a Col_o deep blue mesophase with $Rh^{I}\cdots Rh^{I}$ interactions, a more expanded symmetry, and the anion arranged in the same plane as the cationic unit $[RhL_4]^+$.

Thus, with this exception, all the mesophases of the complexes with L^{D1} or L^{D2} maintain polymeric π-π aryl stacking and Rh···Rh interactions (at somewhat different distances for the two ligands). It is remarkable that in all this complex scaffolding with plenty of π-π stacking of triphenylenes and a large aliphatic continuum, an apparently small detail such as the absence or presence of two Me groups in the isocyanide aryl is decisive for the clearing temperatures and the mesophase ranges of the resulting material, supporting the importance of the π-π stacking of the isocyanide aryls in the Rh complex for the stabilization of whole mesophase building. In contrast with the first pictorial impression in the mesophase illustrations (many red circles of TPh and fewer green circles of RhL_4A) it is the latter the ones that support the formation of this segregated columnar alignment.

The hole mobility of the complexes is two to four orders of magnitude higher than those reported for columnar mesophases formed by triphenylene derivatives only, demonstrating again importance of the columns formed by the metal-containing units. The mobilities measured in the mesophases containing $[Au(CN)_2]^-$ are still one order of magnitude higher than those recorded in the mesophases containing Cl^- or BF_4^-.

Author Contributions

The manuscript has been written through contributions of all authors, who have given approval to this final version of the manuscript.

Conflicts of interest

There are no conflicts to declare.

Acknowledgements

We thank the Spanish MICINN (Project PID2020-118547GB-I00) for financial support, and Dr. Marconi N. Peñas-Defrutos for resolution of the X-ray diffraction structures. V. C.-R. thanks MINECO for a predoctoral FPI studentship.

B.D. and B.H. thank CNRS and the University of Strasbourg for support and Pohang Accelerator Laboratory (PAL) for giving us the opportunity to perform the GIWAXS measurements, MEST and POSTECH for supporting these experiments, Dr. Hyungju Ahn for adjustments and help, and other colleagues from the 9A USAXS beamline for assistance.

R.T. and A.G. thank Franco Cofone of NANOTEC-CNR for helping in samples preparation.

References

1 (a) J. W. Dart, M. K Lloyd, R. Mason and, J. A. McCleverty, *J. Chem. Soc. Dalton Trans*., 1973, 2039; (b) D. Baumann, H. J Kellek, D Nöthe, H. H. Rupp and G. Uhlman,. *Z. Naturforsch, E: Anorg. Chem., Org. Chem*., 1976, **31B**, 912; (c) K. R. Mann, N. S. Lewis, R. M. Williams, H. B.Gray and J. G. Gordon, *Inorg. Chem*., 1978, **17**, 828; (d) Y. Yamamoto, , K. I. Aoki and H. Yamazaki, *Inorg. Chem*., 1979, **18**, 1681; (e) H. Endres, N. Gottstein, H. J. Keller, R. Martin, W. Rodemer and W. Steiger, *Z. Naturforsch, E: Anorg. Chem.,Org. Chem*., 1979, **34B**, 827; (f) K. R. Mann, J. A. Thich, R. A. Bell, C. L. Coyle and H. B. Gray, *Inorg. Chem.,* 1980, **19**, 2462; (g) S. Miya, Y. Yamamoto and H. Yamazaki, *Inorg. Chem*., 1982, **21**, 1486; (h) Y. Yamamoto, Y. Wakatsuki and H. J. Yamazaki, *Organometallics*, 1983, **2**, 1604.

2 S. Grimme and J.-P. Djukic, *Inorg. Chem*., 2011, **50**, 2619.

3 (a) V. W.-W. Yam, V. K.-M. Au, and S. Y.-L.; Leung, *Chem. Rev*., 2015, **115**, 7589, and references therein; (b) A. K.-W. Chan, K. M.-C. Wong and V. W.-W. Yam, *J. Am. Chem. Soc.,* 2015, **137**, 6920.

4 Y. Chen, K. Li, H. O. Lloyd, W. Lu, S. S.-Y. Chui and C.-M. Che, *Angew. Chem. Int. Ed*., 2010, **49**, 9968.

5 T. Tominaga and T. Mochida, *Chem. Eur. J*., 2018, **24**, 6239.

6 H. Ito, T. Kato and M. Sawamura, *Chem. Asian J*., 2007, **2**, 1436.

7 (a) G. Cui, X.-Y. Cao, W.-H. Fang, M. Dolg and W. Thiel, *Angew. Chem. Int. Ed*., 2013, **52**, 10281; (b) M. Iwamura, K. Nozaki, S. Takeuchi and T. Tahara, *J. Am. Chem. Soc*., 2013, **135**, 538; (c) S. R. Hettiarachchi, M. A. Rawashdeh-Omary, S. M. Kanan, M. A. Omary, H. H. Patterson and C. P. Tripp, *J. Phys. Chem. B*, 2002, **106**, 10058; (d) M. A Rawashdeh-Omary, M. A. Omary, H. H. Patterson and J. P. Fackler, *J. Am. Chem. Soc.*, 2001, **123**, 11237;

(e) M. A. Rawashdeh-Omary, M. A., Omary and H. H. Patterson, *J. Am. Chem. Soc.*, 2000, **122**, 10371.

8 (a) Q. Liu, M. Xie, X. Chang, Q. Gao, Y. Chen and W. Lu, *Chem. Commun.*, 2018, **54**, 12844; (b) Q. Liu, M. Xie, X. Chang, S. Cao, C. Zou, W.-F. Fu, C.-M. Che, Y. Chen and W. Lu, *Angew. Chem. Int. Ed.*, 2018, **57**, 6279.

9 M. Barcenilla, C. L. Folcia, J. Ortega, J. Etxebarria, S. Coco and P. Espinet, *J. Mater. Chem. C*, 2022, **10**, 932.

10 V. Conejo-Rodríguez, M. N. Peñas–Defrutos and P. Espinet, *Chem. Commun*., 2019, **55**, 5005.

11 Reviews in journals: (a) P. Espinet, M. A. Esteruelas, L. Oro, J. L. Serrano and E. Sola, *Coord. Chem. Rev.* 1992, **117**, 215. (b) B. Donnio, *Inorg. Chim. Acta*, 2014, **409**, 53.

12 Books and book chapters: (a) Metallomesogens. J. L. Serrano, Ed.; VCH: Weinheim, Germany, 1996. (b) D. W. Bruce, in Inorganic Materials, 2nd ed.; D. W. Bruce, D. O'Hare, Eds.; Wiley: Chichester, U.K. 1996; Chapter 8. (c) B. Donnio, D. Guillon, D. W. Bruce, R. Deschenaux, Metallomesogens, in Comprehensive Organometallic Chemistry III: From Fundamentals to Applications; Crabtree, R. H., Mingos, D. M. P., Eds.; Elsevier: Oxford, U.K., 2006; Vol. 12 (Applications III: Functional Materials, Environmental and Biological Applications), Chapter 12.05, pp 195−294. (d) S. Coco and P. Espinet, Liquid Crystals Based on Gold Compounds. In *Gold Chemistry: Applications and Future Directions in the Life Sciences*; Mohr, F., Ed.; Wiley-VCH Verlag GmbH & CoKGaA:Weiheim, Germany, 2009; pp 357–396.

13 S. Sergeyev, W.; Pisula and Y. H. Geerts, *Chem. Soc. Rev*., 2007, **36**, 1902.

14 (a) Y. Shimizu, A. Kurobe, H. Monobe, N. Terasawa, K. Kiyohara and K. Uchida, *Chem. Commun*., 2003, 1676. (b) R. J. Bushby, N. Boden, C. A. Kilner, O. R. Lozman, Z. Lu, Q. Liu and M. A. Thornton-Pett, *J. Mater. Chem.*, 2003, **13**, 470. (c) T. Kato, N. Mizoshita and K. Kishimoto, *Angew. Chem., Int. Ed*., 2006, **45**, 38. (d) S. Kumar, *Chem. Soc. Rev*., 2006, **35**, 83. (e) S. K. Gupta, V. Raghunathan and S. Kumar, *New. J. Chem*., 2008, **33**, 112. (f). H. K. Bisoyi and S. Kumar, *Tetrahedron Lett*. 2008, **49**, 3628. (g) X. Feng, V. Marcon, W. Pisula, M. R. Hansen, J. Kirkpatrick, F. Grozema, D. Andrienko, K. Kremer and K. Müllen, *Nat. Mater*., 2009, **8**, 421. (h) I. Tahar-Djebbar, F. Nekelson, B. Heinrich, B. Donnio, D. Guillon, D. Kreher, F. Mathevet and A.-J. Attias, *Chem. Mater*., 2011, **23**, 4653. (i) S. Sauer, N. Steinke, A. Baro, S. Laschat, F. Giesselmann and W. Kantlehner, *Chem. Mater*., 2008, **20**, 1909.

15 T. Wöhrle, I. Wurzbach, J. Kirres, A. Kostidou, N. Kapernaum, J. Litterscheidt, J. C. Haenle, P. Staffeld, A. Baro, F. K. Giesselmann and S. Laschat, *Chem. Rev*., 2016, **116**, 1139.

16 (a) C. Tschierske, *Angew. Chem., Int. Ed.*, 2013, **52**, 8828. (b) R. C. Borner, R. J. Bushby, A. N. Cammidge and M. V. Jesudason, *Liq. Cryst*. 2006, **33**, 1439. (c) X. Kong, Z.; He, H. Gopee, X. Jing and A. N. Cammidge, *Tetrahedron Lett.* 2011, **52**, 77. (d) S. K. Varshney, *Liq. Cryst*. 2013, **40**, 1477.

17 (a) S. Kumar, *Liq. Cryst*., 2004, **31**, 1037; (b) S. Kumar, *Liq. Cryst.,* 2005, **32**, 1089.

18 (a) W. Pisula and K. Müllen, Discotic Liquid Crystals as Organic Semiconductors. In Handbook of Liquid Crystals, J. W. Goodby, P. J. Collings, T. Kato, C. Tschierske, H. F. Gleeson and P. Raynes, Eds.; Wiley-VCH: Weinheim, 2014; Vol. 8, pp. 627. (b) S. Dorian and B. Brigitte, *Tetrahedron Letters*, 2019, **60**, 872.

19 (a) W. Pisula, M. Kastler, D. Wasserfallen, M. Mondeshki, J. Piris, I. Schnell and K. Müllen, *Chem. Mater*., 2006, **18**, 3634; (b) M.; O'Neill and S. M. Kelly, *Adv. Mater*., 2003, **15**, 1135; (c) J. Simmerer, B. Glüsen, W. Paulus, A. Kettnwe, P. Schuhmacher, A. Adam, K. H. Etzbach, K. Siemensmeyer, J. H. Wendorff, P. Roisin, G. P. Rigby, R. Nolte, M. J. Cook and S. C. Thorpe, *Sens. Actuators B*, 1993, **13-14**, 276; (d) D. Adam, P. Schuhmacher, J. Simmerer, L. Haussling, K. Siemensmeyer, K. H. Etzbach, H. Ringsdorf and D. Haarer, *Nature*, 1994, **371**, 141.

20 (a) B. Mohr, G. Wegner and K. Ohta, *Chem. Comm*., 1995, 995. (b) J. L. Schulte, S. Laschat, R. Schulte-Ladbeck, V. von Arnim, A. Schneider and H. Finkelmann, *J. Organomet. Chem*., 1998, **552**, 171.

21 (a) S. Kumar and S. K. A Varshney, *Liq. Cryst*., 2001, **28**, 161. (b) A. N. Cammidge and H. Gopee, *Chem. Comm.* 2002, 966.

22 (a) Y. Wang, Y. Liu, J. Luo, H. Qi, X. Li, M. Nin, M. Liu, D. Shi, W. Zhu and Y. Cao, *Dalton Trans*., 2011, 40, 5046. (b) F. Bai, X. Yang, H. Guo and C. Li, *Tetrahedron Lett*., 2013, **54**, 409. (c) J. Shi, Y. Wang, M. Xiao, P. Zhong, Y. Liu, H. Tan, M. Zhu and W. Zhu, *Tetrahedron.,* 2015, **71**, 463.

23 (a) E. Tritto, R. Chico, G. Sanz-Enguita, C. L. Folcia, J. Ortega, S. Coco and P. Espinet, *Inorg. Chem*., 2014, **53**, 3449. (b) E. Tritto, R. Chico, J. Ortega, C. L. Folcia, J. Etxebarria, S. Coco and P. Espinet, *J. Mater. Chem. C.*, 2015, **3**, 9385. (c) R. Chico, C. Domínguez, B. Donnio, B. Heinrich, S. Coco and P. Espinet, *Cryst. Growth Des*., 2016, **16**, 6984. (d) R. Chico, E. de Domingo, C. Domínguez, B. Donnio, B. Heinrich, R. Termine, A. Golemme, S. Coco and P. Espinet, *Chem. Mater*., 2017, **29**, 7587–7595. (e) A. B. Miguel−Coello, M. Bardají, S. Coco, B. Donnio, B. Heinrich and P. Espinet, *Inorg. Chem*., 2018, **57**, 8, 4359. (f) E. Domingo, C. L. Folcia, J. Ortega, J. Etxebarria, R. Termine, A. Golemme, S. Coco and P. Espinet, *Inorg, Chem*., 2020, **59**, 10482.

24 (a) I. Ugi and R. Meyr, *Chem. Ber*., 1960, **93**, 239; (b) W. P. Weber, G. W. Gokel and I. Ugi, *Angew. Chem., Int. Ed. Engl*., 1972, **11**, 530.

25 T. V. Ashworth, D. C. Liles, H. E. Oosthuizen and E. Singleton, *Acta Cryst*., 1984, **C40**, 1169.

26 S. Alvarez, *Dalton Trans*., 2013, ***42***, 8617.

27 (a) K.-Q. Zhao, X.-Y. Bai, B. Xiao, Y. Gao, P. Hu, B.-Q. Wang, Q.-D. Zeng, C. Wang, B. Heinrich and B. Donnio**,** *J. Mater. Chem. C.***,** 2015, **3**, 11735; (b) W. Zhang, W.-H. Yu, C. Feng, S.-K. Xiang, B.-Q. Wang, K.-Q. Zhao, H.-L. Ni and P. Hu, *Liquid Crystals*., 2020, **47**, 1100; (c) A. Herbaut and E. Baranoff, *Chimia*, 2015, **69**, 520.

28 (a) N. S. Lewis, K. R. Mann, J. G. Gordon and H. B. Gray, *J. Am. Chem. Soc*., 1976, **98**, 7461; (b) A. Efraty, I. Feinstein, F. Frolow and L. Wackerle, *J. Am. Chem. Soc*., 1980, **102**, 6343; (c) M. L. Winzenburg, J. A. Kargol and R. J. Angelici, *J. Organomet Chem*., 1983, **249**, 415; (d) A. L. Balch and M. M. Olmstead, *J. Am. Chem. Soc*., 1976, **98**, 2354.

29 (a) K. R. Mann, J. G. Gordon and H. B. Gray, *J. Am. Chem. Soc*., 1975, **97**, 3553. (b) B. E. Bursten and R. F. Fenske, *Inorg. Chem*., 1977, **16**, 963.

30 D. Myśliwiec, B. Donnio, P. J. Chmielewski, B. Heinrich and M. Stępień, *J. Am. Chem. Soc*., 2012, **134**, 4822.

31 (a) M. M.; Ahmida and S. H. Eichhorn, *ECTS Trans.*, 2010, **25**, 1; (b) S. J. Mahoney, M. M. Ahmida, H. Kayal, N. Fox, Y. Shimizucand and S. H. Eichhor, *J. Mater. Chem.*, 2009, **19**, 9221.
32 R. Termine and A. Golemme, *Int. J. Mol. Sci.*, 2021, **22**, 877.
33 B. Feringan, R. Termine, A. Golemme, J.M. Granadino-Roldán, A. Navarro, R. Giménez and T. Sierra, *J. Mater. Chem. C*, 2021, **9**, 1972.

Mesogenic $[Rh(L)_4](A)$ Complexes Form Mesophases with $Rh^I\cdots Rh^I$-Containing and Triphenylene-Discotic Segregated Columns. Effect of $Rh^I\cdots Rh^I$ Interactions and $A^- = [Au(CN)_2]^-$ on Hole Mobility

$[Rh(CNAr)_4](A)$ Rh^I cationic complexes with four polyalkoxytriphenylene-arylisocyanide ligands $\mathbf{L^{D1}}$ and L^{D2} produce deeply coloured mesophases with segregated triphenylene/metal-complex columns in large temperature ranges from –9 to 169 °C, with hole mobilities two to four orders of magnitude higher relative to the hole mobility of purely organic triphenylene columns, and still one more order of magnitude if the anion is $[Au(CN)_2]^-$.